

See discussions, stats, and author profiles for this publication at: <https://www.researchgate.net/publication/51728274>

Nucleoside-Assisted Self-Assembly of Oligo(p-phenylenevinylene)s at Liquid/Solid Interface: Chirality and Nanostructures

ARTICLE in JOURNAL OF THE AMERICAN CHEMICAL SOCIETY · NOVEMBER 2011

Impact Factor: 12.11 · DOI: 10.1021/ja206437c · Source: PubMed

CITATIONS

26

READS

46

11 AUTHORS, INCLUDING:



Zongxia Guo

Qingdao University of Science and Technology

20 PUBLICATIONS 192 CITATIONS

[SEE PROFILE](#)



Bernard Van Averbeke

Université de Mons

19 PUBLICATIONS 547 CITATIONS

[SEE PROFILE](#)



Roberto Lazzaroni

Université de Mons

400 PUBLICATIONS 9,372 CITATIONS

[SEE PROFILE](#)



Albertus P H J Schenning

Technische Universiteit Eindhoven

295 PUBLICATIONS 14,398 CITATIONS

[SEE PROFILE](#)

Nucleoside-Assisted Self-Assembly of Oligo(*p*-phenylenevinylene)s at Liquid/Solid Interface: Chirality and Nanostructures

Zongxia Guo,[†] Inge De Cat,[†] Bernard Van Averbeke,[§] Jianbin Lin,[‡] Guojie Wang,^{†,||} Hong Xu,[†] Roberto Lazzaroni,^{*,§} David Beljonne,[§] E. W. Meijer,[‡] Albertus P. H. J. Schenning,^{*,‡} and Steven De Feyter^{*,†}

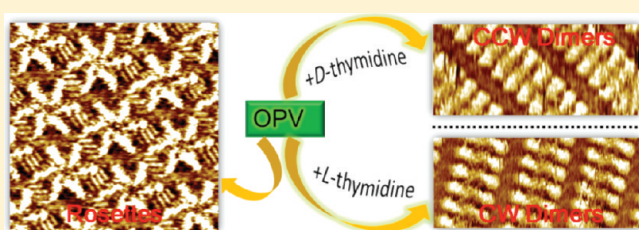
[†]Division of Molecular Imaging and Photonics, Department of Chemistry, Katholieke Universiteit Leuven (K.U. Leuven), Celestijnlaan 200 F, B-3001 Leuven, Belgium

[‡]Laboratory of Macromolecular and Organic Chemistry, Eindhoven University of Technology, P.O. Box 513, 5600 MB Eindhoven, The Netherlands

[§]Service de Chimie des Matériaux Nouveaux, Université de Mons, Place du Parc 20, 7000 Mons, Belgium

Supporting Information

ABSTRACT: The formation of DNA nucleoside-assisted π -conjugated nanostructures was studied by means of scanning tunneling microscopy (STM) and force field simulations. Upon adsorption of the achiral oligo(*p*-phenylenevinylene) (OPV) derivative at the liquid/solid interface, racemic conglomerates with mirror related rosettes are formed. Addition of the DNA nucleosides D- and L-thymidine, which act as “chiral handles”, has a major effect on the supramolecular structure and the expression of chirality of the achiral OPV molecules. The influence of these “chiral handles” on the expression of chirality is probed at two levels: monolayer symmetry and monolayer orientation with respect to the substrate. This was further explored by tuning the molar ratio of the building blocks. Molecular modeling simulations give an atomistic insight into the monolayer construction, as well as the energetics governing the assembly. Thymidine is able to direct the chirality and the pattern of OPV molecules on the surface, creating chiral lamellae of π -conjugated dimers.



INTRODUCTION

Functional materials at surfaces,^{1–10} in particular biobased structures, have received increasing attention because of their specific recognition and self-organization abilities and their possible use in devices such as sensors and advanced drug deliveries.^{11–23}

Not only biomolecules but also π -conjugated compounds have great potential, as nanostructures formed by the self-assembly of those molecules can be used in organic electronics.^{24–31} Among π -conjugated systems, oligo(*p*-phenylenevinylene) (OPV) derivatives are of particular interest, and their self-assembly process into supramolecular architectures and the resulting properties have been examined thoroughly.^{32–41}

By combining specific recognition with organic electronics, a new research approach in the fabrication of functional materials emerged: biomolecule-assisted supramolecular assembly of π -conjugated molecules.^{42–48} This approach resembles nature’s concept in which templates with specific binding sites are used to efficiently form well-defined assemblies. Combining π -conjugated molecules with biomolecules is an attractive approach to obtain nanostructures having a well-defined size and geometry and positional control.⁴⁹ Such hybrid materials show not only recognition ability but also fine electronic and optical properties, which might enhance the performance of light-harvesting

systems and nanoelectronic devices based on organic semiconductors.^{50–58} A necessary condition for the predominance of biomolecule-assisted assembly over self-assembly is that the free energy change resulting from the combined effects of biomolecule–molecule and biomolecule-assisted molecule–molecule interactions is larger than the free energy gain from the self-assembly of the molecules themselves.

Here, we report on a new development in this field: the induction of supramolecular surface-confined architectures of π -conjugated oligomers, that is, OPV molecules, by nucleosides at the liquid/solid interface. We studied the self-assembly of such a nucleoside and a π -conjugated OPV oligomer building block into hybrid chiral architectures at the liquid/solid interface using scanning tunneling microscopy (STM) as the imaging tool. Inspired by hydrogen-bonding interactions prevailing in biological systems, we have selected thymidine (Figure 1, both enantiomers), which is one of the DNA nucleosides, as the biomolecule building block and an achiral OPV with a diaminotriazine hydrogen bonding unit (A-OPV3T, Figure 1) as the π -conjugated system. The complementary hydrogen-bonding interaction between A-OPV3T and thymidine was

Received: July 11, 2011

Published: October 18, 2011

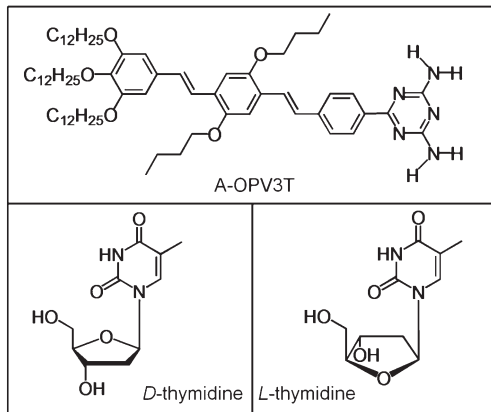


Figure 1. Molecular structures of A-OPV3T, D-thymidine and L-thymidine.

anticipated to be an attractive way to create and control the chiral supramolecular organization of the π -conjugated oligomers at the liquid/solid interface.^{45–48} Addition of a second component can induce a structural transformation of the self-assembled structures and even homochirality if the molecules added are chiral.^{59–63} Playing with the molecular ratio can help to control the self-assembly of these multicomponent organic structures.^{64–66}

We characterized the structure and chirality of self-assembled monolayers of A-OPV3T and of A-OPV3T/thymidine complexes at the 1-octanol/HOPG interface by using STM, which is an excellent tool to investigate the molecular self-assembly and dynamics of supramolecular architectures at surfaces or interfaces with submolecular resolution.^{67–76} The self-assembly of various DNA nucleobases has already been studied at the liquid/solid interface with STM.^{77–80} Likewise, the self-assembly of several OPV-derivatives is documented.^{32–36,81} However, combining both types of molecules brings new and interesting perspectives. It was found that A-OPV3T self-assembles into chiral cyclic hexamers and forms a racemic conglomerate. By premixing with enantiopure thymidine, chiral lamellae of π -conjugated dimers were observed, revealing a dramatic change in the two-dimensional architecture and an intriguing complex expression of surface chirality. Molecular modeling simulations provided additional insight in the monolayer structure. These results show that nucleosides can be used to direct the ordering of π -conjugated molecules.

■ RESULTS AND DISCUSSION

Self-Assembly of A-OPV3T at the 1-Octanol/HOPG Interface. In the first phase, we studied the self-assembly of A-OPV3T at the 1-octanol/HOPG interface by means of STM (Figure 2). Similar to other 1,3-diaminotriazine-functionalized OPV derivatives,^{35,36,81} A-OPV3T formed a well-defined monolayer composed of hydrogen-bonded cyclic hexamers, so-called rosettes. Two types of rosettes, related by mirror-image symmetry, were found, as shown in Figure 2a. We identify the rosettes as clockwise (CW) and counterclockwise (CCW) on the basis of the relative orientation of the OPV units in line with previous assignments. The bright rods correspond to the conjugated OPV backbone because of the high local density of states, while the dodecyloxy chains are dark due to the lower local density of states.^{82,83} More than 95% of the monolayer consists of rosette structures, and the relative contribution of CW and

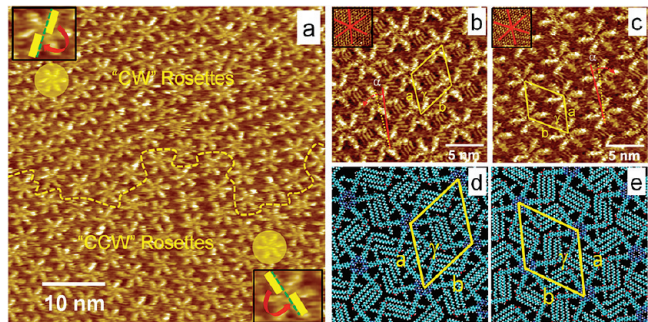


Figure 2. STM images of A-OPV3T at the 1-octanol/HOPG interface. (a) $I_{\text{set}} = 0.28$ nA, $V_{\text{set}} = -0.30$ V. Insets highlight the structure of clockwise (CW) and counterclockwise (CCW) rosettes. The yellow dashed line separates a CW and a CCW rosette domain. Yellow rods cover OPV units to show where the OPV is located. (b) CW rosettes: $I_{\text{set}} = 0.28$ nA, $V_{\text{set}} = -0.40$ V. (c) CCW rosettes: $I_{\text{set}} = 0.70$ nA, $V_{\text{set}} = -0.28$ V. Insets in (b) and (c) are images of HOPG, recorded underneath the corresponding monolayers. In (b) and (c), the red solid lines reflect the main symmetry axes of the graphite. The yellow dotted lines run parallel to the unit cell vector a . [A-OPV3T] = 1.0 mM. Tentative models of the A-OPV3T monolayer structure with CW rosettes (d) and CCW rosettes (e) are shown, and a unit cell is indicated in yellow for each model.

CCW rosettes is about the same. In addition to defects (4%), a small amount of dimers (<1%) is formed (Supporting Information S1).

Figure 2b,c shows high-resolution images of a domain of CW and CCW rosettes, respectively. The unit cell parameters were measured as: $a = 5.5 \pm 0.2$ nm, $b = 5.6 \pm 0.1$ nm, $\gamma = 61 \pm 1^\circ$ for CW rosettes, and $a = 5.5 \pm 0.1$ nm, $b = 5.4 \pm 0.1$ nm, $\gamma = 60 \pm 2^\circ$ for CCW rosettes. Not surprisingly, the unit cell parameters are the same within experimental error. Models for the CW and CCW rosettes were made on the basis of previous reports (Figure 2d,e, and Supporting Information S2).^{35,36} A rosette consists of six OPV molecules held together by hydrogen bonds. The van der Waals interactions between interdigitated alkyl chains of neighboring rosettes, the hydrogen bonds in the center of the rosettes, and the molecule–substrate interactions stabilize the monolayer at the liquid/solid interface. High-resolution STM images reveal that only two out of three dodecyloxy chains per OPV unit are adsorbed on the HOPG surface. The other dodecyloxy chain extends into the bulk solution. The adsorbed alkyl chains align along the normal to the main graphite symmetry axes ($11\bar{2}0$).

Achiral molecules often self-assemble into chiral supramolecular structures at the liquid/solid interface.^{84–86} This is also the case for the assembly of A-OPV3T at the 1-octanol/HOPG interface. The pattern formed by A-OPV3T belongs to plane group $p6$, one of the five chiral plane groups.⁶⁷ Furthermore, A-OPV3T assembles into a monolayer composed of different rosette domains, which have opposite orientations (CW rosette domain, -9° ; CCW rosette domain, $+10^\circ$) with respect to the main symmetry axis of the underlying HOPG substrate. Thus, chirality is not only expressed at the level of the monolayer symmetry, but also by the relative orientation of the monolayer with respect to the substrate underneath. Similar results have been reported for related achiral OPV derivatives.⁸¹

Thymidine-Assisted Self-Assembly of A-OPV3T. To study the influence of nucleosides on the nanostructures formed by A-OPV3T molecules at the liquid/solid interface, we used thymidine (D- and L-thymidine) as a chiral handle. There is no

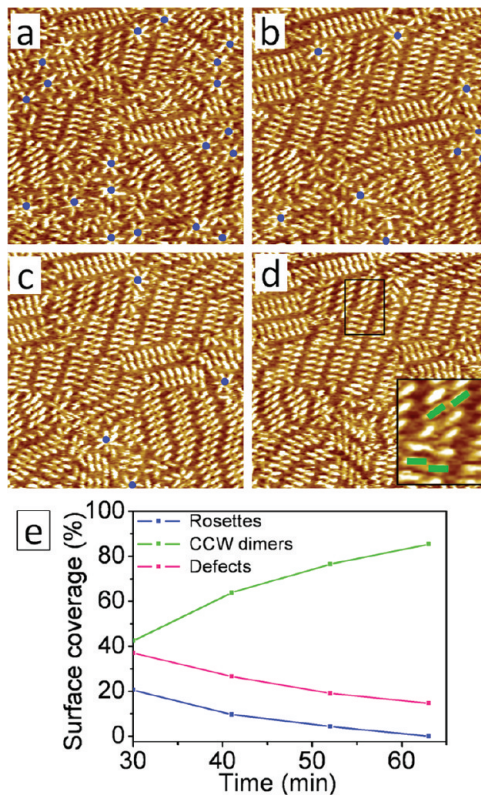


Figure 3. (a–d) Sequence of STM images of A-OPV3T in the presence of d-thymidine ($R = [\text{d-thymidine}]:[\text{A-OPV3T}] = 0.5$) with a time interval of 11 min. The first image was recorded 30 min after dropcasting. $[\text{A-OPV3T}] = 1.0 \text{ mM}$. $I_{\text{set}} = 0.50 \text{ nA}$, $V_{\text{set}} = -0.25 \text{ V}$. Image size is $42 \times 42 \text{ nm}$. Blue disks indicate rosettes. Inset in (d) is a magnification of the area indicated with a black rectangle. Two dimers are indicated with green rods. Each colored unit corresponds to an A-OPV3T molecule. (e) Surface coverage (%) of rosettes, CCW dimers, and defects as a function of time.

evidence for the adsorption of pure thymidine into a monolayer at the 1-octanol/HOPG interface. To influence the self-assembly of A-OPV3T, A-OPV3T and thymidine were premixed in solution.

A droplet of a mixture of d-thymidine and A-OPV3T with a d-thymidine/A-OPV3T molar ratio (R) of 0.5 was applied onto the substrate. STM imaging was started quickly after dropcasting, and the first stable image was obtained after 30 min. A dynamic transformation from rosettes as observed in Figure 2 to so-called “dimers”, which are aligned in rows, was clearly visualized (Figure 3). In analogy with the rosettes, each bright rod in such a dimer is attributed to an OPV backbone. These images provide no information on the location of the thymidine molecules. A detailed discussion on the composition of these new supramolecular structures and the role of the thymidine molecules follows later. All of the dimers were oriented counterclockwise (CCW), defined as the direction of the dimers against the normal of the row axis. Because this process was monitored within a short time period, the effect of solvent evaporation could be neglected. The STM images were recorded at the same location as a function of time (Supporting Information S3). Four distinct images were chosen to illustrate the time-dependent changes.

We calculated the number of A-OPV3T molecules forming rosettes and the number of A-OPV3T molecules forming CCW

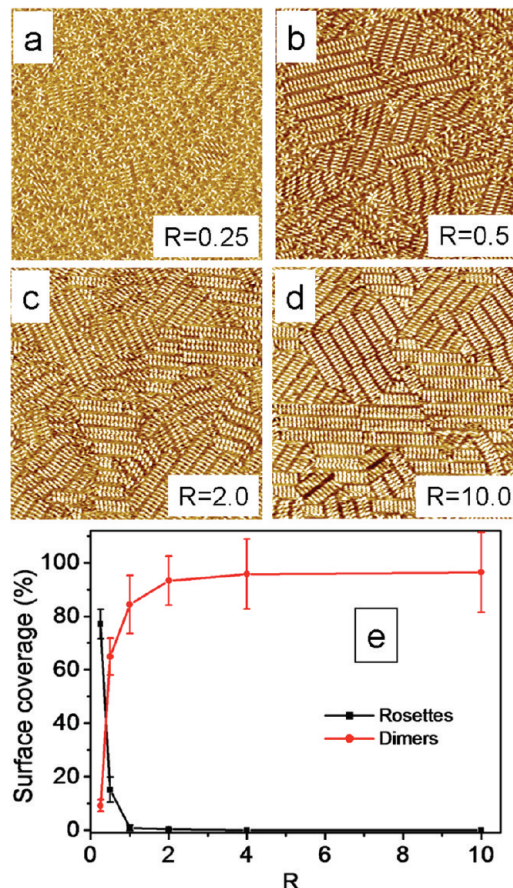


Figure 4. Molar ratio-dependent pattern transformation of A-OPV3T at the 1-octanol/HOPG interface with the addition of d-thymidine. $R = [\text{d-thymidine}]:[\text{A-OPV3T}]$, $[\text{A-OPV3T}] = 1.0 \text{ mM}$. (a) $R = 0.25$, $I_{\text{set}} = 0.25 \text{ nA}$, $V_{\text{set}} = -0.23 \text{ V}$. (b) $R = 0.5$, $I_{\text{set}} = 0.50 \text{ nA}$, $V_{\text{set}} = -0.25 \text{ V}$. (c) $R = 2.0$, $I_{\text{set}} = 0.285 \text{ nA}$, $V_{\text{set}} = -0.208 \text{ V}$. (d) $R = 10.0$, $I_{\text{set}} = 0.500 \text{ nA}$, $V_{\text{set}} = -0.269 \text{ V}$. STM image size is $80 \times 80 \text{ nm}$. (e) Surface coverage of rosettes and dimers as a function of R .

dimers. Figure 3e shows the change in surface coverage of rosettes, dimers, and defects. The surface coverage of both rosettes and defects decreased over time, while that of CCW dimers increased accordingly. So, both rosettes and defects gradually turned into CCW dimers. This means that the dimers are the thermodynamically most stable packing and that the defects are healed in time, creating a more regular monolayer. After approximately 1 h, a total amount of 85% dimers were found on the surface. Because measurements after 90 min and more also gave a value of approximately 85% (Figure 4), we can state that the curve starts to level off after 1 h, reaching an equilibrium.

This shows that thymidines are able to interact with A-OPV3T molecules inducing a time-dependent pattern transformation from rosettes to dimers. Dimers proved to be more stable than rosettes. To ensure that the equilibrium is reached and to avoid dynamics for further measurements, the molecules were left to self-assemble at least 90 min prior to STM imaging.

The interaction with thymidine was then further studied by looking at mixtures of A-OPV3T and d-thymidine with different molar ratios keeping the concentration of A-OPV3T constant (Figure 4). Upon increasing the concentration of d-thymidine with respect to A-OPV3T, rosettes disappear at the benefit of dimers. For

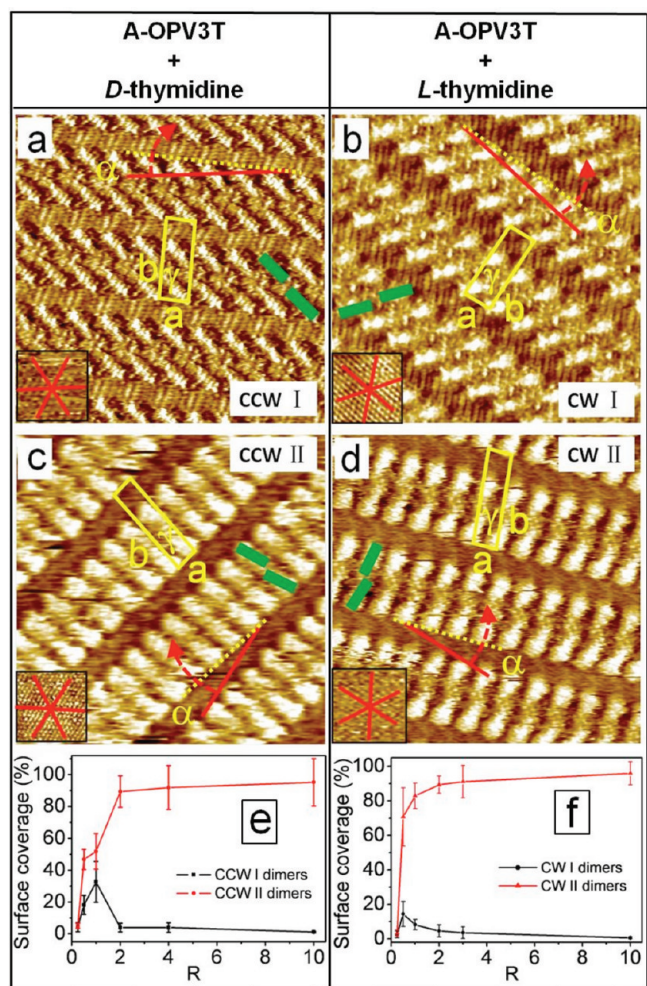


Figure 5. STM images of (a) A-OPV3T with D-thymidine, $I_{\text{set}} = 0.45$ nA, $V_{\text{set}} = -0.24$ V. (b) A-OPV3T with L-thymidine, $I_{\text{set}} = 0.35$ nA, $V_{\text{set}} = -0.25$ V. (c) A-OPV3T with D-thymidine, $I_{\text{set}} = 1.0$ nA, $V_{\text{set}} = -0.25$ V. (d) A-OPV3T with L-thymidine, $I_{\text{set}} = 0.189$ nA, $V_{\text{set}} = -0.302$ V. Insets are STM images of the graphite substrate underneath the respective monolayers. In (a)–(d), red solid lines reflect the symmetry axes of graphite. Yellow dotted lines run parallel to the unit cell vector a . The relative orientation of the OPV units within one dimer is highlighted in green. Size of all images is 18×18 nm. (e and f) Surface coverage of type I and type II dimers as a function of R with [A-OPV3T] = 1.0 mM.

$R = 0.25$, only a few dimer structures could be found on the surface. At very high molar ratios of thymidine (e.g., $R = 10$), the rosettes have completely disappeared, and the monolayer consists almost exclusively of dimers (97%). At $R = 1$, the curve shows an inflection point, suggesting a 1:1 hydrogen-bonded complexation between thymidine and the diaminotriazine unit of A-OPV3T.

Moreover, when looking more closely into the dimer structures, two kinds of dimers could be found. Both dimers are CCW for the combination of A-OPV3T and D-thymidine, but the packing is different. The dimers, so-called CCW I and CCW II, are shown in Figure 5a and b, respectively. The CCW dimer unit cell parameters are: $a = 1.8 \pm 0.1$ nm, $b = 4.8 \pm 0.1$ nm, $\gamma = 89 \pm 3^\circ$ for CCW I, and $a = 1.6 \pm 0.1$ nm, $b = 5.6 \pm 0.1$ nm, $\gamma = 84 \pm 3^\circ$ for CCW II. Both unit cells belong to the chiral $p2$ plane group.^{87,88}

For the combination of A-OPV3T and L-thymidine, there is a similar molar ratio-dependent structural transformation from

rosettes to dimers (Supporting Information S4). In this case, two types of CW dimers are formed, as shown in Figure 5c and d.⁸⁹ The dimer unit cell parameters are characterized as: $a = 1.7 \pm 0.1$ nm, $b = 4.7 \pm 0.1$ nm, $\gamma = 89 \pm 2^\circ$ for CW I, and $a = 1.5 \pm 0.1$ nm, $b = 5.6 \pm 0.2$ nm, $\gamma = 86 \pm 4^\circ$ for CW II. The CW I and CCW I, and CW II and CCW II patterns are enantiomorphous; that is, they are mirror images. Furthermore, the orientations of the monolayer with respect to the main symmetry axes of the underlying HOPG are opposite for CCW I ($+9^\circ$) and CW I (-10°), and also for CCW II ($+17^\circ$) and CW II (-18°).

There are similar differences between type I and type II dimers based on CW and CCW patterns: (i) type II has a smaller a vector and a larger b vector; (ii) the angle between the long axis of a type II dimer and the normal of the lamella direction is smaller than that for type I dimers; and (iii) most of the alkyl chains between two lamella were too fuzzy to be resolved in STM images for type II as compared to type I, in which two out of three alkyl chains per OPV unit are physisorbed and can be easily resolved in STM images.

In addition, the relative amount of type I dimers with respect to type II dimers changes with increasing R (thymidine: A-OPV3T). At very low R , for example, $R = 0.25$ for D-thymidine, an equal amount of CCW I and CCW II is formed on the surface, while for $R = 0.5$, an obvious preference for CCW II dimers is found. Figure 5e shows the variation in surface coverage for CCW I and CCW II dimers as a function of R . When R is smaller than 0.5, the surface coverages of CCW I and CCW II both increase with increasing R . When R is larger than 0.5, the surface coverage of CCW I starts to decrease, while that of CCW II continues increasing with increasing R . For R higher than 1, the surface coverage of CCW II starts to level off. For example, when $R = 10$, the surface coverage of CCW II is 95%, while that of CCW I is smaller than 1%. So, the structural transformation is molar ratio dependent and CCW II is the dominant structure for a mixture of A-OPV3T and D-thymidine. For a mixture of A-OPV3T and L-thymidine, similar results were obtained (Figure 5f), but the dominant structure is now the CW II dimer.

As discussed above, the addition of thymidine to a solution of A-OPV3T leads to the emergence of dimer structures at the liquid/solid interface. This pattern transformation indicates that thymidine interacts with A-OPV3T through noncovalent interactions adsorbing in or on top of the A-OPV3T layer. When the unit cell parameters of type I and type II dimers formed by A-OPV3T mixed with thymidine were compared to those of the dimers formed by pure A-OPV3T, a significantly different b value was found (Supporting Information S1). This difference indicates that the thymidine molecules interacting with A-OPV3T molecules are not on top of the monolayer but coadsorbed with A-OPV3T on the substrate. The expression of chirality also suggests that thymidine interacts and is part of the monolayer: thymidines with opposite chirality led to dimers with opposite chirality. Chirality is not only expressed at the level of the pattern structure but also at the level of the monolayer with respect to the basal plane of HOPG. Thus, the chirality of thymidine directs the chirality of the self-assembled monolayer. Taking spatial hindrance into account, thymidine can only take one way and be partly coadsorbed on the surface. Accordingly, to form complex via complementary hydrogen bondings with thymidines, A-OPV3T can adsorb on the surface by one way. Basically, the chirality of the chiral center in thymidine exerts steric interaction to OPV molecules.

To check if there are interactions between the two components in solution, NMR experiments were carried out using a solution that was also used for the STM experiments. The experimental data (Supporting Information S6) showed no interaction between A-OPV3T and thymidine. In other words, no hydrogen bond is formed between A-OPV3T and thymidine in solution, prior to adsorption on the surface. Because there is a pattern transformation and change in chirality after addition of thymidine at the liquid/solid interface, the substrate must play a crucial role and drive the interactions. Therefore, the liquid/solid 2D constraint must be of key importance.^{90–92}

Modeling of A-OPV3T/Thymidine Dimers. A Molecular Mechanics/Molecular Dynamics (MM/MD) approach was used to shed light on the possible structural arrangements of the supramolecular dimers formed by A-OPV3T and L-thymidine (we expect the A-OPV3T/d-thymidine dimers to show mirror-imaged structures). In these simulations, the A-OPV3T/thymidine ratio used is 1:1, based on the assumption of coadsorption on the surface and complementarity of hydrogen-bonding sites.

Initial structures were built on the basis of assembly models inspired from the STM results. It is important to stress that the formation of a dense adlayer on graphite is incompatible with all of the dodecyloxy side chains of the OPV cores lying flat on the surface. The STM measurements indicate that one of the three side chains is completely desorbed from the surface and solvated by 1-octanol molecules for the CW I and CCW I dimers. Because explicit solvent molecules are not considered in our calculations, we simply removed one of the three dodecyloxy chains from each A-OPV3T core for the sake of simplicity. As described below, the other two chains partially adsorb on the graphite surface, thereby contributing to the formation of the adlayer.

Models for monolayers including 16 A-OPV3T and 16 L-thymidine molecules were generated on top of a double layer of graphite. The calculations were carried out with frozen lattice

parameters, which are in agreement with the corresponding STM values. The resulting structures are shown in Figure 6.

In the CW I dimer (left column), the axes of the conjugated backbones of the two OPV units belonging to neighbor dimers are almost perfectly aligned, with the two thymidine molecules located in front of the diaminotriazine groups and back-to-back with respect to each other (Figure 6a). This geometry has the following consequence on the size and shape of the unit cell: due to the sterical hindrance between thymidines and the OPV side chains on the central ring, the short axis value is larger with respect to that observed in CW II. As a consequence, the space available between OPV molecules is large enough to allow for partial interdigitation of the long terminal alkyl chains, resulting in the CW I pattern represented in Figure 6a. In the CW II dimer (right column), the OPV backbones are clearly shifted with respect to each other. Again, one thymidine molecule is located in front of each diaminotriazine unit, but, due to the shift between the conjugated backbones, each thymidine molecule can also interact laterally with the other OPV molecule (Figure 6b). Such a lateral interaction, combined with the absence of sterical hindrance between the thymidines and the alkyl groups on the central ring of the OPV unit, results in a smaller interstitial space between the OPV molecules. The long axis thus elongates with respect to what is observed for CW I, so as to reduce the repulsion between the long alkyl chains, giving the CW II arrangement in Figure 6b.

The influence of constraining the lattice parameters of the assembly to their STM values is clearly visible in the region between OPV rows, which features a higher degree of configurational disorder and partial or total desorption of the alkyl chains from the surface (this is illustrated in the side views at the bottom of Figure 6). To quantify this effect, we have estimated the desorption ratio, D , of those chains by integrating the radial distribution function of the corresponding carbon atoms above

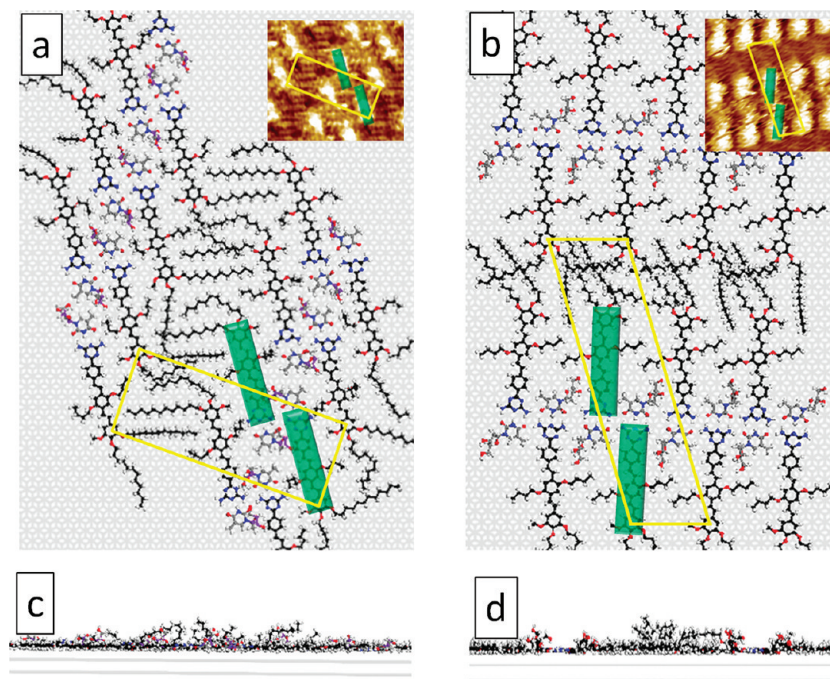


Figure 6. Models for the monolayers of the CW I (left) and CW II (right) dimers on graphite. (a and b) Top view of the assemblies; (c and d) Side view of the assemblies. Nitrogen atoms in blue and oxygen atoms in red. Insets in (a) and (b) were zoomed in from Figure 5 b and d and then rotated in the plane with a proper angle. A yellow unit cell and an OPV dimer (where one green rectangle covers one OPV unit) were both shown in (a), (b), and the zoomed-in STM images.

a certain cutoff distance from the surface (5 Å, Supporting Information S7). For model CW I, we obtain a desorption ratio of 0.26, indicating that on average 9 out of the 12 carbon atoms are in contact with the graphite surface in each dodecyl chain. In model CW II, the desorption ratio is larger ($D \approx 0.35$); that is, on average only 8 carbon atoms per dodecyl chain are in contact with the surface. This more pronounced desorption of the alkyl chains yields a more disordered arrangement, which is consistent with the increased fuzziness in the STM images for type II dimers.

It thus appears that the A-OPV3T/thymidine system preferentially arranges into monolayers (CW I and CW II) with a dense molecular packing but disordered, partially desorbed alkyl chains, rather than in a “more classical”, more ordered structure with full adsorption of the alkyl chains but a less dense packing. To understand that behavior, we have compared the energetics of the adsorption on graphite for the CW I and CW II layers and for hypothetical structures in which the alkyl chains are allowed to fully adsorb. The total interaction energy per dimer, which is mostly driven by molecule–surface interactions (Supporting Information Table S8), is larger in those hypothetical assemblies, because of the more favorable CH– π contacts between graphite and the alkyl chains. However, when examining the total energy per unit surface area, this is compensated by the smaller area occupied by each dimer in the dense “disordered” assembly, which is found to be the most stable: about -43 kcal mol $^{-1}$ dimer $^{-1}$ nm $^{-2}$ for the dense “disordered” assembly versus about -36 kcal mol $^{-1}$ dimer $^{-1}$ nm $^{-2}$ for the ordered, less dense structure (Supporting Information Table S8). Thus, the system spontaneously evolves into a trade-off situation where the alkyl chains are still significantly bound to the graphite surface but partly desorbed to maximize the monolayer density. This trend is expected to be even more favorable in the real situation, in which the desorbed parts of the alkyl chains are further stabilized by solvation, a process that is not taken into account in the modeling.

The total interaction energies per dimer between the CW I and CW II structures are very close: -42.87 kcal mol $^{-1}$ dimer $^{-1}$ nm $^{-2}$ for CW I versus -43.20 kcal mol $^{-1}$ dimer $^{-1}$ nm $^{-2}$ for CW II. These values result from a trade-off between larger molecule–molecule interactions in CW II (hydrogen bonding and Coulomb interactions) and better CH– π interactions with the surface for CW I (see Supporting Information Table S8 for details). Such a similarity between the total interaction energies can explain the fact that both types of arrangements can coexist on the surface; the very small difference in favor of CW II is consistent with the prevalence of that structure when the amount of thymidine increases (i.e., when the A-OPV3T/thymidine ratio is close or larger than 1). Note that the molecule–molecule interactions are more clearly in favor of CW II, which further supports the formation of that type of assembly.

CONCLUSIONS

The self-assembly of A-OPV3T, and the thymidine-induced self-assembly of A-OPV3T, were systematically studied at the 1-octanol/HOPG interface by STM and modeling tools. A-OPV3T can form an ordered racemic conglomerate monolayer composed of CW and CCW rosette domains. In a mixture of A-OPV3T with thymidine, A-OPV3T interacts with thymidine on the surface by hydrogen bonding, although there is no interaction between these two building blocks in solution, under

the experimental conditions used for self-assembly at the liquid/solid interface. A thymidine-induced morphological change of the A-OPV3T monolayer pattern was observed. Enantiomorphous dimers were obtained from A-OPV3T with D-thymidines and A-OPV3T with L-thymidines. The chirality of the dimers and the monolayer was dominated by the chirality of thymidine. An overall chiral monolayer was induced by the introduction of thymidine enantiomers. The thymidines play a key role in not only the chiral expression but also the surface packing. The control of surface packing and chiral expression of A-OPV3T was realized by changing the molar ratio of both components. With the assistance of molecular modeling simulations, type II dimers were found to be the dominant superstructures by evaluating the adsorption energy per unit area, which is in agreement with the STM measurements. Controlling the chiral supramolecular organization of π -conjugated molecules by using (oligo)nucleotides is an appealing approach to create well-defined 2D supramolecular patterns, which is of importance in the fields of molecular recognition and (nano)electronic devices.

The present research can give new insights into the assembly of biological/conjugated molecules in the use of organic electronic devices as well: First, it expands the concept from DNA strand-templated to nucleoside-induced or further nucleobase-induced assembly; second, the moieties with complementary sites can be reversed in principle, and superstructure features and properties could be further exploited; and third, not only the binding group but also the conjugated unit can be replaced, that is, other nucleobases or nucleosides as binding groups, and other conjugated systems such as oligothiophene derivatives as conjugated backbone.

EXPERIMENTAL SECTION

Synthesis. Details of the synthesis of A-OPV3T were reported before.⁹³ D-Thymidine and L-thymidine were bought from Carbosynth and used as received.

Scanning Tunneling Microscopy. All experiments were carried out at 20–25 °C. Experiments were performed using a PicoSPM microscope (Agilent). Tips were mechanically cut from Pt–Ir wire (80:20 alloy, diameter 0.25 mm). Prior to imaging, the A-OPV3T and/or the thymidines were dissolved in 1-octanol (Anhydrous, 99+%, Sigma-Aldrich), and a drop of this solution was applied onto a freshly cleaved surface of highly oriented pyrolytic graphite (HOPG, grade ZYB, Advanced Ceramics Inc., Cleveland, OH). Almost all of the STM imaging started at least 90 min after dropcasting to avoid interference of the initial dynamics at the liquid/solid interface. Images were recorded in the constant current mode. V_{set} refers to the sample bias. The graphite lattice was recorded by lowering the sample bias immediately after obtaining images of the monolayer. Drift effects were corrected via scanning probe image processor (SPIP) software (Image Metrology ApS).

Molecular Modeling. The physisorption of the adlayers on graphite was modeled by means of a Molecular Mechanics/Molecular Dynamics (MM/MD) approach. The DREIDING force field,⁹⁴ as implemented in the FORCITE tool pack of Materials Studio, was used, because it is particularly adapted to account for the hydrogen bonds that promote the self-assembly of the molecules. To validate the force field for the estimation of adsorption energies, we have considered a series of alkane molecules, for which experimental data are available in literature.⁹⁵ The energies obtained with DREIDING are in close agreement with those experimental values, which validates the choice of this force field here. The force field calculations were performed on model systems including A-OPV3T and L-thymidine molecules in a 1:1 ratio deposited on graphite. The initial geometric configurations were

inspired from assembly models based on the STM measurements. These were then subjected to energy minimization at 0 K, releasing step by step all constraints imposed during the construction of the assemblies, followed by MD simulations in the NVT ensemble at 298 K for 1 ns. The long-range nonbonded interactions were turned off with a cubic spline cutoff set at 18 Å.

■ ASSOCIATED CONTENT

S Supporting Information. STM images, NMR spectra, and molecular modeling. This material is available free of charge via the Internet at <http://pubs.acs.org>.

■ AUTHOR INFORMATION

Corresponding Author

roberto.lazzaroni@umons.ac.be; a.p.h.j.schenning@tue.nl; steven.defeyter@chem.kuleuven.be

Present Addresses

[†]University of Science and Technology Beijing.

■ ACKNOWLEDGMENT

This work was supported by the European Commission through the Marie Curie Research Training Network CHEXTAN (MRTN-CT-2004-512161) and the RESOLVE project (NMP4-SL-2008-214340), by the Interuniversity Attraction Pole program of the Belgian Federal Science Policy Office (PAI 6/27), by the Fund of Scientific Research—Flanders (FWO), and the Institute for the Promotion of Innovation by Science and Technology in Flanders (IWT). Research in Mons is also supported by Région Wallonne (OPTI2MAT excellence program) and FNRS-FRFC. D.B. is an FNRS research director.

■ REFERENCES

- (1) Barth, J. V.; Costantini, G.; Kern, K. *Nature* **2005**, *437*, 671–679.
- (2) Tauk, L.; Schröder, A. P.; Decher, G.; Giuseppone, N. *Nat. Chem.* **2009**, *1*, 649–656.
- (3) Love, J. C.; Estroff, L. A.; Kriebel, J. K.; Nuzzo, R. G.; Whitesides, G. M. *Chem. Rev.* **2005**, *105*, 1103–1170.
- (4) Tao, F.; Bernasek, S. L.; Xu, G. Q. *Chem. Rev.* **2009**, *109*, 3991–4024.
- (5) Wen, Y.; Liu, Y.; Guo, Y.; Yu, G.; Hu, W. *Chem. Rev.* **2011**, *111*, 3358–3406.
- (6) Wu, D.; Liu, R.; Pisula, W.; Feng, X.; Müllen, K. *Angew. Chem., Int. Ed.* **2011**, *50*, 2791–2794.
- (7) Maday, T. E.; Pelhos, K.; Wu, Q.; Barnes, R.; Ermanoski, I.; Chen, W.; Kolodziej, J. J.; Rowe, J. E. *Proc. Natl. Acad. Sci. U.S.A.* **2002**, *99*, 6503–6508.
- (8) Loo, Y.-L.; Willett, R. L.; Baldwin, K. W.; Rogers, J. A. *Appl. Phys. Lett.* **2002**, *81*, 562–564.
- (9) Haes, A. J.; Van Duyne, R. P. *J. Am. Chem. Soc.* **2002**, *124*, 10596–10604.
- (10) Nie, Z.; Kumacheva, E. *Nat. Mater.* **2008**, *7*, 277–290.
- (11) Stevens, M. M.; George, J. H. *Science* **2005**, *310*, 1135–1138.
- (12) Wong, L. S.; Khan, F.; Micklefield, J. *Chem. Rev.* **2009**, *109*, 4025–4053.
- (13) Dickerson, M. B.; Sandhage, K. H.; Naik, R. R. *Chem. Rev.* **2008**, *108*, 4935–4978.
- (14) Whaley, S. R.; English, D. S.; Hu, E. L.; Barbara, P. F.; Belcher, A. M. *Nature* **2000**, *405*, 665–668.
- (15) Rogero, C.; Chaffey, B. T.; Mateo-Martí, E.; Sobrado, J. M.; Horrocks, B. R.; Houlton, A.; Lakey, J. H.; Briones, C.; Martín-Gago, J. A. *J. Phys. Chem. C* **2008**, *112*, 9308–9314.
- (16) Seeman, N. C.; Belcher, A. M. *Proc. Natl. Acad. Sci. U.S.A.* **2002**, *99*, 6451–6455.
- (17) Seeman, N. C. *Nature* **2003**, *421*, 427–431.
- (18) Comellas-Aragones, M.; Engelkamp, H.; Claessen, V. I.; Sommerdijk, N. A. J. M.; Rowan, A. E.; Christianen, P. C. M.; Maan, J. C.; Verduin, B. J. M.; Cornelissen, J. J. L. M.; Nolte, R. J. M. *Nat. Nanotechnol.* **2007**, *2*, 635–639.
- (19) Capito, R. M.; Azevedo, H. S.; Velichko, Y. S.; Mata, A.; Stupp, S. I. *Science* **2008**, *319*, 1812–1816.
- (20) Stupp, S. I. *Nano Lett.* **2010**, *10*, 4783–4786.
- (21) Vos, M. R. J.; Breurken, M.; Leclerc, P. E. L. G.; Bomans, P. H. H.; de Haas, F.; Frederik, P. M.; Jansen, J. A.; Nolte, R. J. M.; Sommerdijk, N. A. J. M. *J. Am. Chem. Soc.* **2008**, *130*, 12608–12609.
- (22) Kershner, R. J.; Bozano, L. D.; Micheel, C. M.; Hung, A. M.; Fornof, A. R.; Cha, J. N.; Rettner, C. T.; Bersani, M.; Frommer, J.; Rothemund, P. W. K.; Wallraff, G. M. *Nat. Nanotechnol.* **2009**, *4*, 557–561.
- (23) Zhang, S. *Nat. Biotechnol.* **2003**, *21*, 1171–1178.
- (24) Hoeben, F. J. M.; Jonkheijm, P.; Meijer, E. W.; Schenning, A. P. H. *J. Chem. Rev.* **2005**, *105*, 1491–1546.
- (25) Meijer, E. W.; Schenning, A. P. H. *J. Nature* **2002**, *419*, 353–354.
- (26) Watson, M. D.; Fechtenkötter, A.; Müllen, K. *Chem. Rev.* **2001**, *101*, 1267–1300.
- (27) Grimsdale, A. C.; Müllen, K. *Angew. Chem., Int. Ed.* **2005**, *44*, 5592–5629.
- (28) Wu, J.; Pisula, W.; Müllen, K. *Chem. Rev.* **2007**, *107*, 718–747.
- (29) Bauert, T.; Merz, L.; Bandera, D.; Parschau, M.; Siegel, J. S.; Ernst, K.-H. *J. Am. Chem. Soc.* **2009**, *131*, 3460–3461.
- (30) Wang, J.; Kulago, A.; Browne, W. R.; Feringa, B. L. *J. Am. Chem. Soc.* **2010**, *132*, 4191–4196.
- (31) Palermo, V.; Otten, M. B. J.; Liscio, A.; Schwartz, E.; de Witte, P. A. J.; Castricano, M. A.; Wienk, M. M.; Nolde, F.; De Luca, G.; Cornelissen, J. J. L. M.; Janssen, R. A. J.; Müllen, K.; Rowan, A. E.; Nolte, R. J. M.; Samorí, P. *J. Am. Chem. Soc.* **2008**, *130*, 14605–14614.
- (32) De Feyter, S.; Miura, A.; Yao, S.; Chen, Z.; Würthner, F.; Jonkheijm, P.; Schenning, A. P. H. J.; Meijer, E. W.; De Schryver, F. C. *Nano Lett.* **2005**, *5*, 77–81.
- (33) Gesquiere, A.; Jonkheijm, P.; Hoeben, F. J. M.; Schenning, A. P. H. J.; De Feyter, S.; De Schryver, F. C.; Meijer, E. W. *Nano Lett.* **2004**, *4*, 1175–1179.
- (34) Hoeben, F. J. M.; Zhang, J.; Lee, C. C.; Pouderoijen, M. J.; Wolffs, M.; Würthner, F.; Schenning, A. P. H. J.; Meijer, E. W.; De Feyter, S. *Chem.-Eur. J.* **2008**, *14*, 8579–8589.
- (35) Jonkheijm, P.; Miura, A.; Zdanowska, M.; Hoeben, F. J. M.; De Feyter, S.; Schenning, A. P. H. J.; De Schryver, F. C.; Meijer, E. W. *Angew. Chem., Int. Ed.* **2004**, *43*, 74–78.
- (36) Miura, A.; Jonkheijm, P.; De Feyter, S.; Schenning, A. P. H. J.; Meijer, E. W.; De Schryver, F. C. *Small* **2005**, *1*, 131–137.
- (37) Uji-i, H.; Miura, A.; Schenning, A.; Meijer, E. W.; Chen, Z. J.; Würthner, F.; De Schryver, F. C.; Van der Auweraer, M.; De Feyter, S. *ChemPhysChem* **2005**, *6*, 2389–2395.
- (38) Schenning, A. P. H. J.; Meijer, E. W. *Chem. Commun.* **2005**, 3245–3258.
- (39) Chen, Q.; Chen, T.; Wang, D.; Liu, H. B.; Li, Y. L.; Wan, L. J. *Proc. Natl. Acad. Sci. U.S.A.* **2010**, *107*, 2769–2774.
- (40) González-Rodríguez, D.; Janssen, P. G. A.; Martín-Rapún, R.; De Cat, I.; De Feyter, S.; Schenning, A. P. H. J.; Meijer, E. W. *J. Am. Chem. Soc.* **2010**, *132*, 4710–4719.
- (41) Jonkheijm, P.; van der Shoot, P.; Schenning, A. P. H. J.; Meijer, E. W. *Science* **2006**, *313*, 80–83.
- (42) Jatsch, A.; Schillingerl, E.-K.; Schmid, S.; Bäuerle, P. *J. Mater. Chem.* **2010**, *20*, 3563–3578.
- (43) Janssen, P. G. A.; Meeuwenoord, N.; van der Marel, G.; Jabbari-Farouji, S.; van der Schoot, P.; Surin, M.; Tomović, Ž.; Meijer, E. W.; Schenning, A. P. H. *J. Chem. Commun.* **2010**, *46*, 109–111.
- (44) Ruiz-Carretero, A.; Janssen, P. G. A.; Kaeser, A.; Schenning, A. P. H. *J. Chem. Commun.* **2011**, *47*, 4340–4347.

- (45) Ruiz-Carretero, A.; Janssen, P. G. A.; Stevens, A. L.; Surin, M.; Herz, L. M.; Schenning, A. P. H. *J. Chem. Commun.* **2011**, *47*, 884–886.
- (46) Janssen, P. G. A.; Vandenberghe, J.; van Dongen, J. L. J.; Meijer, E. W.; Schenning, A. P. H. *J. Am. Chem. Soc.* **2007**, *129*, 6078–6079.
- (47) Iwaura, R.; Hoeben, F. J. M.; Masuda, M.; Schenning, A. P. H. J.; Meijer, E. W.; Shimizu, T. *J. Am. Chem. Soc.* **2006**, *128*, 13298–13304.
- (48) Surin, M.; Janssen, P. G. A.; Lazzaroni, R.; Leclerc, P.; Meijer, E. W.; Schenning, A. P. H. *Adv. Mater.* **2009**, *21*, 1126–1130.
- (49) Kumar, R. J.; MacDonald, J. M.; Singh, T. B.; Waddington, L. J.; Holmes, A. B. *J. Am. Chem. Soc.* **2011**, *133*, 8564–8573.
- (50) Matmour, R.; De Cat, I.; George, S. J.; Adriaens, W.; Leclerc, P.; Bomans, P. H. H.; Sommerdijk, N. A. J. M.; Gielen, J. C.; Christianen, P. C. M.; Heldens, J. T.; van Hest, J. C. M.; Löwik, D. W. P. M.; De Feyter, S.; Meijer, E. W.; Schenning, A. P. H. J. *J. Am. Chem. Soc.* **2008**, *130*, 14576–14583.
- (51) Nilsson, K. P. R.; Rydberg, J.; Baltzer, L.; Inganäs, O. *Proc. Natl. Acad. Sci. U.S.A.* **2003**, *100*, 10170–10174.
- (52) Nilsson, K. P. R.; Rydberg, J.; Baltzer, L.; Inganäs, O. *Proc. Natl. Acad. Sci. U.S.A.* **2004**, *101*, 11197–11202.
- (53) Frauenrath, H.; Jahnke, E. *Chem.-Eur. J.* **2008**, *14*, 2942–2955.
- (54) Jatsch, A.; Kopyshev, A.; Mena-Osteritz, E.; Bäuerle, P. *Org. Lett.* **2008**, *10*, 961–963.
- (55) Klok, H.-A.; Rösler, A.; Götz, G.; Mena-Osteritz, E.; Bäuerle, P. *Org. Biomol. Chem.* **2004**, *2*, 3541–3544.
- (56) Diegelmann, S. R.; Gorham, J. M.; Tovar, J. D. *J. Am. Chem. Soc.* **2008**, *130*, 13840–13841.
- (57) Schillinger, E.-K.; Mena-Osteritz, E.; Hentschel, J.; Börner, H. G.; Bäuerle, P. *Adv. Mater.* **2009**, *21*, 1562–1567.
- (58) Stone, D. A.; Hsu, L.; Stupp, S. I. *Soft Matter* **2009**, *5*, 1990–1993.
- (59) Ciesielski, A.; Palma, C. A.; Bonini, M.; Samori, P. *Adv. Mater.* **2010**, *22*, 3506–3520.
- (60) Surin, M.; Samori, P. *Small* **2007**, *3*, 190–194.
- (61) Langner, A.; Tait, S. L.; Lin, N.; Rajadurai, C.; Ruben, M.; Kern, K. *Proc. Natl. Acad. Sci. U.S.A.* **2007**, *104*, 17927–17930.
- (62) Parschau, M.; Romer, S.; Ernst, K. H. *J. Am. Chem. Soc.* **2004**, *126*, 15398–15399.
- (63) Humblot, V.; Lorenzo, M. O.; Baddeley, C. J.; Haq, S.; Raval, R. *J. Am. Chem. Soc.* **2004**, *126*, 6460–6469.
- (64) Palma, C. A.; Bjork, J.; Bonini, M.; Dyer, M.; Llanes-Pallas, A.; Bonifazi, D.; Persson, M.; Samori, P. *J. Am. Chem. Soc.* **2009**, *5*, 13062–13071.
- (65) Huang, Y. L.; Chen, W.; Li, H.; Ma, J.; Pflaum, J.; Wee, A. T. S. *Small* **2010**, *6*, 70–75.
- (66) Sun, X.; Jonkman, H. T.; Silly, F. *Nanotechnology* **2010**, *21*, 165602–165607.
- (67) Plass, K. E.; Grzesiak, A. L.; Matzger, A. J. *Acc. Chem. Res.* **2007**, *40*, 287–293.
- (68) Gutzler, R.; Sirtl, T.; Dienstmaier, J. F.; Mahata, K.; Heckl, W. M.; Schmittel, M.; Lackinger, M. *J. Am. Chem. Soc.* **2010**, *132*, 5084–5090.
- (69) Madueno, R.; Räisänen, M. T.; Silien, C.; Buck, M. *Nature* **2008**, *454*, 618–621.
- (70) Ceres, D. M.; Barton, J. K. *J. Am. Chem. Soc.* **2003**, *125*, 14964–14965.
- (71) Cyr, D. M.; Venkataraman, B.; Flynn, G. W. *Chem. Mater.* **1996**, *8*, 1600–1615.
- (72) Yuan, Q. H.; Yan, C. J.; Yan, H. J.; Wan, L. J.; Northrop, B. H.; Jude, H.; Stang, P. J. *J. Am. Chem. Soc.* **2008**, *130*, 8878–8879.
- (73) Smith, D. P. E.; Horber, J. K. H.; Binnig, G.; Nejoh, H. *Nature* **1990**, *344*, 641–644.
- (74) De Feyter, S.; Gesquiere, A.; Abdel-Mottaleb, M. M.; Grim, P. C. M.; De Schryver, F. C.; Meiners, C.; Sieffert, M.; Valiyaveettil, S.; Müllen, K. *Acc. Chem. Res.* **2000**, *33*, 520–531.
- (75) Askadskaya, L.; Rabe, J. P. *Phys. Rev. Lett.* **1992**, *69*, 1395–1398.
- (76) Liu, L.; Zhang, L.; Mao, X.; Niu, L.; Yang, Y.; Wang, C. *Nano Lett.* **2009**, *9*, 4066–4072.
- (77) Mamdouh, W.; Dong, M. D.; Xu, S. L.; Raols, E.; Besenbacher, F. *J. Am. Chem. Soc.* **2006**, *128*, 13305–13311.
- (78) Xu, S. L.; Dong, M. D.; Raols, E.; Otero, R.; Linderoth, T. R.; Besenbacher, F. *Nano Lett.* **2006**, *6*, 1434–1438.
- (79) Mamdouh, W.; Kelly, R. E. A.; Dong, M. D.; Kantorovich, L. N.; Besenbacher, F. *J. Am. Chem. Soc.* **2008**, *130*, 695–702.
- (80) Ciesielski, A.; Lena, S.; Masiero, S.; Spada, G. P.; Samori, P. *Angew. Chem., Int. Ed.* **2010**, *49*, 1–8.
- (81) Katsonis, N.; Xu, H.; Haak, R. M.; Kudernac, T.; Tomovic, Z.; George, S.; Van der Auweraer, M.; Schenning, A. P. H. J.; Meijer, E. W.; Feringa, B. L.; De Feyter, S. *Angew. Chem., Int. Ed.* **2008**, *47*, 4997–5001.
- (82) Mcgonigal, G. C.; Bernhardt, R. H.; Thomson, D. J. *Appl. Phys. Lett.* **1990**, *57*, 28–30.
- (83) Lazzaroni, R.; Calderone, A.; Bredas, J. L.; Rabe, J. P. *J. Chem. Phys.* **1997**, *107*, 99–105.
- (84) Wei, Y. H.; Kannappan, K.; Flynn, G. W.; Zimmt, M. B. *J. Am. Chem. Soc.* **2004**, *126*, 5318–5322.
- (85) Tao, F.; Bernasek, S. L. *J. Phys. Chem. B* **2005**, *109*, 6233–6238.
- (86) Merz, L.; Guntherodt, H.; Scherer, L. J.; Constable, E. C.; Housecroft, C. E.; Neuburger, M.; Hermann, B. A. *Chem.-Eur. J.* **2005**, *11*, 2307–2318.
- (87) Lei, S. B.; Wang, C.; Yin, S. X.; Wang, H. N.; Xi, F.; Liu, H. W.; Xu, B.; Wan, L. J.; Bai, C. L. *J. Phys. Chem. B* **2001**, *105*, 10838–10841.
- (88) Plass, K. E.; Kim, K.; Matzger, A. J. *J. Am. Chem. Soc.* **2004**, *126*, 9042–9053.
- (89) Note that when A-OPV3T was mixed with equal amounts of both thymidine enantiomers, the ratio between CW and CCW dimers was the same (Supporting Information S5).
- (90) Elemans, J. A. A. W.; De Cat, I.; Xu, H.; De Feyter, S. *Chem. Soc. Rev.* **2009**, *38*, 722–736.
- (91) Iavicoli, P.; Xu, H.; Feldborg, L. N.; Linares, M.; Paradinas, M.; Stafstrom, S.; Ocal, C.; Nieto-Ortega, B. L.; Casado, J.; Navarrete, J. T. L.; Lazzaroni, R.; De Feyter, S.; Amabilino, D. B. *J. Am. Chem. Soc.* **2010**, *132*, 9350–9362.
- (92) De Feyter, S.; De Schryver, F. C. *Chem. Soc. Rev.* **2003**, *32*, 139–150.
- (93) Wolfs, M.; George, S. J.; Tomovic, Z.; Meskers, S. C. J.; Schenning, A. P. H. J.; Meijer, E. W. *Angew. Chem., Int. Ed.* **2007**, *46*, 8203–8205.
- (94) Mayo, S. L.; Olafson, B. D.; Goddard, W. A. *J. Phys. Chem.* **1990**, *94*, 8897–8909.
- (95) Paserba, K. R.; Gellman, A. J. *Phys. Rev. Lett.* **2001**, *86*, 4338–4341.